Atmospheric
Chemistry
and Physics

Kinetics of the OH + NO$_2$ reaction: rate coefficients (217–333 K, 16–1200 mbar) and fall-off parameters for N$_2$ and O$_2$ bath gases

Damien Amedro, Arne J. C. Bunkan, Matias Berasategui, and John N. Crowley

Division of Atmospheric Chemistry, Max-Planck-Institut für Chemie, 55128 Mainz, Germany

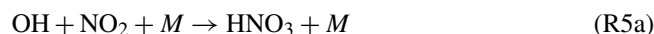**Correspondence:** John N. Crowley (john.crowley@mpic.de)

Abstract. The radical terminating, termolecular reaction between OH and NO$_2$ exerts great influence on the NO$_y$/NO$_x$ ratio and O$_3$ formation in the atmosphere. Evaluation panels (IUPAC and NASA) recommend rate coefficients for this reaction that disagree by as much as a factor of 1.6 at low temperature and pressure. In this work, the title reaction was studied by pulsed laser photolysis and laser-induced fluorescence over the pressure range 16–1200 mbar and temperature range 217–333 K in N$_2$ bath gas, with experiments at 295 K (67–333 mbar) for O$_2$. In situ measurement of NO$_2$ using two optical absorption set-ups enabled generation of highly precise, accurate rate coefficients in the fall-off pressure range, appropriate for atmospheric conditions.

We found, in agreement with previous work, that O$_2$ bath gas has a lower collision efficiency than N$_2$ with a relative collision efficiency to N$_2$ of 0.74. Using the Troe-type formulation for termolecular reactions we present a new set of parameters with $k_0(\mathrm{N}_2) = 2.6 \times 10^{-30}$ cm^6 molecule^{-2} s^{-1}, $k_0(\mathrm{O}_2) = 2.0 \times 10^{-30}$ cm^6 molecule^{-2} s^{-1}, $m = 3.6$, $k_\infty = 6.3 \times 10^{-11}$ cm^3 molecule^{-1} s^{-1}, and $F_c = 0.39$ and compare our results to previous studies in N$_2$ and O$_2$ bath gases.

1 Introduction

The capacity of the atmosphere to oxidize trace gases and thus cleanse itself of pollutant emissions depends on the availability of OH radicals, which initiate the degradation of many organic and inorganic trace gases (Lelieveld et al., 2004; Lelieveld et al., 2016). Two reactions, the photolysis of ozone in the presence of water vapour (Reactions R1 and R2) and the reaction of HO$_2$ radicals with NO (Reaction R3), are responsible for a large fraction of atmospheric OH production.

$$\mathrm{O}_3 + h\nu \rightarrow \mathrm{O}(^1\mathrm{D}) + \mathrm{O}_2 \tag{R1}$$

$$\mathrm{O}(^1\mathrm{D}) + \mathrm{H}_2\mathrm{O} \rightarrow 2\mathrm{OH} \tag{R2}$$

$$\mathrm{HO}_2 + \mathrm{NO} \rightarrow \mathrm{OH} + \mathrm{NO}_2 \tag{R3}$$

NO$_2$ is a key component in controlling atmospheric oxidation as it contributes via its photolysis (Reaction R4) to formation of tropospheric O$_3$ but also, via the title reaction (Reaction R5), leads to removal of OH.

$$\mathrm{NO}_2 + h\nu\,(\mathrm{O}_2) \rightarrow \mathrm{NO} + \mathrm{O}_3 \tag{R4}$$

$$\mathrm{OH} + \mathrm{NO}_2 + M \rightarrow \mathrm{HNO}_3 + M \tag{R5a}$$
$$\rightarrow \mathrm{HOONO} + M \tag{R5b}$$

Atmospheric HO$_x$ levels (HO$_x$ = OH + HO$_2$) and NO$_x$ levels (NO$_x$ = NO + NO$_2$), from the boundary layer to the stratosphere, are strongly influenced by the radical terminating reaction (Reaction R5) between the hydroxyl radical (OH) and nitrogen dioxide (NO$_2$). Reaction R5 is complex, with its rate coefficient displaying both a pressure and temperature dependence and two different reaction pathways, leading to either nitric acid (HNO$_3$) or pernitrous acid (HOONO). HNO$_3$ is the dominant product under atmospheric conditions and its long lifetime with respect to reformation of OH and NO$_2$ (via reaction with OH or photolysis) and rapid deposition to surfaces in the boundary layer mean that Reaction R5 is effectively a sink of both OH and NO$_2$. The yield of HOONO increases as a function of pressure, with a value of $\sim 14\%$ at atmospheric pressure ($T = 298$ K) (Golden et al., 2003; Hippler et al., 2002; Mollner et al., 2010). The fate of HOONO is thought to be dominated by

thermal decomposition at temperatures typical of the mid-latitude boundary layer, with the reaction with OH and photolysis potentially contributing at higher altitudes and lower temperatures where its thermal lifetime is longer. The impact of the title reaction as a HO$_x$ and NO$_x$ sink thus depends on the relative efficiency of formation of HNO$_3$ and HOONO and the fate of HOONO, investigation of which is beyond the scope of this study.

Whilst the importance of the reaction between OH and NO$_2$ has been recognized for a long time, and is reflected in the numerous studies of the kinetics of this process (see e.g. evaluations of the kinetic data; Atkinson et al., 2006; Burkholder et al., 2015; IUPAC, 2019), a recent modelling study has indicated that uncertainties in the rate coefficient have a great impact on the simulated chemical composition of the atmosphere (Newsome and Evans, 2017). The recommended parameterizations of the independent, expert evaluation panels, IUPAC (IUPAC, 2019) and NASA (Burkholder et al., 2015), for the rate coefficient (k_5) of the title reaction deviate to an unacceptable extent given the importance of this reaction. Figure 1 illustrates how the ratio of the rate coefficients recommended by IUPAC and NASA ($k_5^{\mathrm{IUPAC}}/k_5^{\mathrm{NASA}}$) varies with altitude, and thus pressure and temperature. Up to the tropopause (~ 10 km at mid-latitudes), the difference between k_5^{IUPAC} and k_5^{NASA} is about 10 % but this increases to 60 % at an altitude of 30 km where the pressure and temperature of the stratosphere are low. The lack of consensus between the IUPAC and NASA panels (drawing from the same laboratory-derived datasets) reflects, in part, the complexity of the reaction, the study of which requires coverage of parameter space (pressure and temperature) that demands the use of different experimental methods. Reaction R5 is an association reaction (termolecular process) and the pressure and temperature dependence stems from stabilization of the initially formed association complex, which can dissociate back to reactants at low pressure or proceed to formation of products at high pressure. These types of reactions are generally parameterized using so-called fall-off curves (Troe, 1983, 2012), which require measurement of the rate coefficients at the low- and high-pressure limits, k_0 and k_∞ respectively. The form of the transition between the low-pressure limit, at which the rate coefficient is roughly proportional to pressure, and the high-pressure limit, at which the association complex is fully stabilized, is characterized by a broadening parameter, F_c. The low- and high-pressure limits have to be characterized experimentally, whereas the broadening factor can be estimated (Cobos and Troe, 2003). The IUPAC and NASA evaluation panels take different approaches to the broadening factor, with IUPAC quoting values that vary between ~ 0.3 and 0.6 and NASA taking the more pragmatic approach of fixing F_c at 0.6, which may be justified in many circumstances given the uncertainties associated with k_∞ (see below). We show later that, for the OH + NO$_2$ reaction, the data are better parameterized using a value of F_c close to the theoretical value of 0.39.
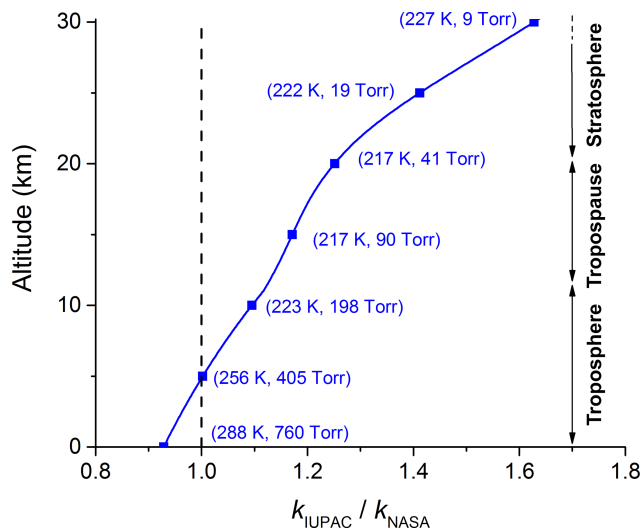
Figure 1. Ratio of the parameterized IUPAC and NASA rate coefficients (k_5) at various altitudes (temperatures and pressures).

The difficulty in parameterizing the rate coefficient for the reaction between OH and NO$_2$ lies in the fact that, across the range of temperatures and pressures that prevail in our atmosphere, the reaction is in the fall-off regime, yet the high-pressure limit is not accessible with standard methods. We show later that experiments conducted at pressures as high as 500 bar He are still below the high-pressure limit and that experiments at pressures as low as 5 Torr N$_2$ (1 Torr = 1.33 mbar = 133 Pa) are already impacted by fall-off. Only three previous studies (Anastasi and Smith, 1976; D'Ottone et al., 2001; Mollner et al., 2010) have determined the rate coefficient at pressures close to 1 bar. Further complexity is added by the fact that the efficiency of collisional deactivation of the association complex is, in contrast to the overwhelming majority of termolecular reactions of atmospheric relevance, different for N$_2$ and O$_2$, the major atmospheric "third-body" bath gases (M in Reaction R5).
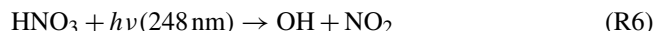
The overall aim of this research was to reduce the uncertainty associated with the rate coefficient in N$_2$ and O$_2$ by generating an additional highly accurate dataset over a wide range of pressures and temperatures relevant for the atmosphere. To do this we have used the pulsed laser photolysis and laser-induced-fluorescence technique coupled with in situ measurement of NO$_2$ concentrations. We note that the rate coefficients we obtain represent the total loss rate coefficient (k_5) for OH loss (i.e. the sum of k_{5a} and k_{5b}).

2 Experimental details

2.1 PLP-LIF technique

Rate coefficients for the title reaction were measured using pulsed laser photolysis (PLP) for generation of OH and laser-induced fluorescence (LIF) to detect it in real time. The details of the experimental set-up have been published previously (Wollenhaupt et al., 2000) and only a brief description is given here. The experiments were carried out in a quartz reactor of volume $\sim 500\,\text{cm}^3$, which was thermostatted to the desired temperature by circulating a 60 : 40 mixture of ethylene glycol / water or ethanol through an outer jacket. The pressure in the reactor was monitored with 100 and 1000 Torr capacitance manometers (MKS). For all experiments, the axial flow velocity in the reactor was kept roughly constant at $\sim 10\,\text{cm}\,\text{s}^{-1}$ by adjusting the flow rate from 270 and 9900 cm^3 (STP) min^{-1} (sccm). As the $\sim 8\,\text{mm}$ wide laser beam was normal to the direction of flow, this ensured that a fresh gas sample was available for photolysis at each laser pulse (laser frequency $= 10\,\text{Hz}$). We additionally carried out some experiments at a lower repetition rate (5 Hz) to help rule out any influence of product build-up on the measured rate coefficient.

Pulses of 248 nm laser light ($\sim 20\,\text{ns}$) for OH generation from HNO$_3$ and H$_2$O$_2$ precursors were provided by an excimer laser (Compex 205 F, Coherent) operated using KrF.

$$\text{HNO}_3 + h\nu(248\,\text{nm}) \rightarrow \text{OH} + \text{NO}_2 \tag{R6}$$

$$\text{H}_2\text{O}_2 + h\nu(248\,\text{nm}) \rightarrow 2\text{OH} \tag{R7}$$

Laser fluences were measured using a calibrated joule meter located behind the exit window of the reactor.

The concentrations of H$_2$O$_2$ and HNO$_3$ were typically in the range 5–10 $\times 10^{13}$ and 5–10 $\times 10^{14}$ molecule cm^{-3} respectively, which, when combined with laser fluences of 5–40 mJ cm^{-2} per pulse, resulted in initial OH concentrations of ~ 1–12×10^{11} molecule cm^{-3}. We show later that variation in the initial radical concentration in this range had no effect on the results obtained, as expected for this chemical system.

OH fluorescence was detected using a photomultiplier tube screened by a 309 nm interference filter and a BG 26 glass cut-off filter following excitation of the OH $A^2\Sigma(v' = 1) \leftarrow X^2\Pi(v'' = 0)$ transition (Q11(1)) at 281.997 nm using a YAG-pumped dye laser (Quantel Brilliant B and Lambda Physik Scanmate). The time-dependent fluorescence signal was accumulated using a boxcar integrator triggered at different delay times between OH formation and excitation.

A second fluorescence detection axis was set up to enable detection of NO$_2$ in the same volume as OH. NO$_2$ was excited at $\sim 564\,\text{nm}$ (Rhodamine 6G dye pumped by a frequency-doubled YAG at 532 nm) and the resulting fluorescence emission was detected using a multi-alkali photomultiplier tube screened by a 605 nm long-pass filter. The boxcar gate was timed to discriminate laser-scattered light from the NO$_2$ fluorescence. The NO$_2$ LIF signal was normalized to laser power using a photodiode sampling a fraction of the excitation pulse.

2.2 Online absorption measurement of NO$_2$ concentration

The experiments to determine the rate coefficient of the title reaction were performed under pseudo-first-order conditions (i.e. $[\text{NO}_2]_0 \gg [\text{OH}]_0$). As a result, the overall uncertainty in k_5 was determined largely by the accuracy with which the NO$_2$ concentration was measured. Depending on the experimental conditions (T, p, and bath gas), the NO$_2$ concentration was varied from 1 to 45×10^{14} molecule cm^{-3}.

The NO$_2$ concentration was continuously measured using two optical absorption cells at room temperature. In the first, upstream of the reactor, absorption of light (405–440 nm) from the collimated output from a halogen lamp transversed a 110 cm long absorption cell before being dispersed with a 0.5 m monochromator (B & M Spektronik BM50, 600 grooves per millimetre, blaze at 500 nm) and detected by a diode-array detector (Oriel InstaSpec 2). The effective spectral resolution ($\delta\lambda = 0.19\,\text{nm}$) of the monochromator–detector set-up was obtained by measuring the width and line shape (Gaussian) of the 404.66 nm Hg line from a low-pressure Hg lamp. NO$_2$ concentrations were determined by fitting optical densities (ODs) from 405 to 440 nm to a reference spectrum (Vandaele et al., 2002) (see Sect. 3.1), which was degraded to the resolution of our spectrometer. The second optical absorption cell (dual beam for simultaneous measurement of transmitted and reference light intensity, 43.8 cm long) was located downstream of the reactor. Here the extinction of 365 nm light from a low-pressure Hg lamp screened using a $365 \pm 5\,\text{nm}$ interference filter was used to continuously monitor NO$_2$ at this wavelength.

The effective NO$_2$ cross section at 365 nm (σ_{365}; see Sect. 3.2) was determined by simultaneously monitoring the NO$_2$ concentration in the first absorption cell and measuring 365 nm extinction in the second absorption cell. σ_{365} was calculated using the Beer–Lambert law:

$$\text{OD}_{365} = \ln\left(\frac{I_0}{I}\right) = \sigma_{365}\,[\text{NO}_2]\,l, \tag{1}$$

where l is the optical path length (43.8 cm) and I_0 and I are the transmitted light intensities at 365 nm in the absence and in the presence of NO$_2$ respectively. The limit of detection of NO$_2$ (defined as 2σ of the signal in the absence of absorbent) was determined to be $\sim 1 \times 10^{13}$ molecule cm^{-3} for both the single wavelength (365 nm) and broadband (405–440 nm) absorption measurements. Drifts in zero measurements result in the smallest measurable OD in the 365 nm cell of $\sim 1 \times 10^{-4}$, which is equivalent to 4.0×10^{12} molecule cm^{-3} NO$_2$.

A third optical absorption cell ($\lambda = 184.95\,\text{nm}$, $l = 40.0\,\text{cm}$) was also used to measure optical extinction by NO$_2$ in experiments in which we explored the effect of pressure

on σ_{NO_2}. Light at 184.95 nm was provided by a low-pressure Hg lamp screened by a 185 ± 5 nm interference filter and was detected using a dual-beam set-up similar to that operated at 365 nm.

2.3   Chemicals

N$_2$ and O$_2$ (Westfalen 99.999 %) were used without further purification. H$_2$O$_2$ (AppliChem, 50 wt %) was concentrated to > 90 % (wt) by vacuum distillation. Anhydrous nitric acid was prepared by mixing KNO$_3$ (Sigma Aldrich, 99 %) and H$_2$SO$_4$ (Roth, 98 %), and condensing HNO$_3$ vapour into a liquid nitrogen trap. NO$_2$ was generated via the reaction of NO with a large excess of O$_2$. The NO$_2$ thus was trapped in liquid N$_2$ and the excess O$_2$ was pumped out. The resulting NO$_2$ was stored as a mixture of ~ 0.5 % NO$_2$ in N$_2$ or ~ 5.5 % NO$_2$ in He. NO (3.5 Air Liquide) was purified of higher NO$_x$ compounds by fractional vacuum distillation.

3   Results and discussion

3.1   NO$_2$ concentration measurement

As NO$_2$ concentrations were monitored in situ by optical absorption at 365 nm, the cross section determination was centrally important for derivation of the rate coefficient and considerable effort was dedicated to its accurate determination, with special attention paid to its pressure dependence.

3.1.1   Pressure dependence of the NO$_2$ absorption cross section at 365 nm

NO$_2$ has a complex and highly structured absorption spectrum in the UV–visible region with band shapes and line intensities depending on both temperature and pressure (Atkinson et al., 2004; IUPAC, 2019). The atomic Hg lines, used to determine [NO$_2$] in this work, are very narrow and therefore pressure broadening of NO$_2$ lines around 365 nm could affect the retrieved concentration. We performed two experiments (at room temperature) that indicate that, from 20 to 800 Torr of N$_2$, any pressure dependence in the NO$_2$ absorption cross section at 365 nm can safely be neglected.

In the first experiment, we simultaneously monitored optical extinction due to a flowing sample of NO$_2$ in N$_2$ at 184.95 and 365 nm. Whereas the NO$_2$ spectrum around 365 nm is highly structured (corresponding to excitation from the ground electronic state to the $(1)^2 B_2$ state), in the vacuum UV (180–220 nm) the spectrum obtained following excitation to the $(2)^2 B_2$ electronic state is largely continuous in nature (Au and Brion, 1997). It is highly unlikely that any pressure broadening effects for these two transitions/spectral regions will be identical. Figure 2a displays the result of a series of experiments in which the optical density (OD) observed for NO$_2$ concentrations between 2×10^{14} and 4×10^{15} molecule cm^{-3} at three different pressures (20,
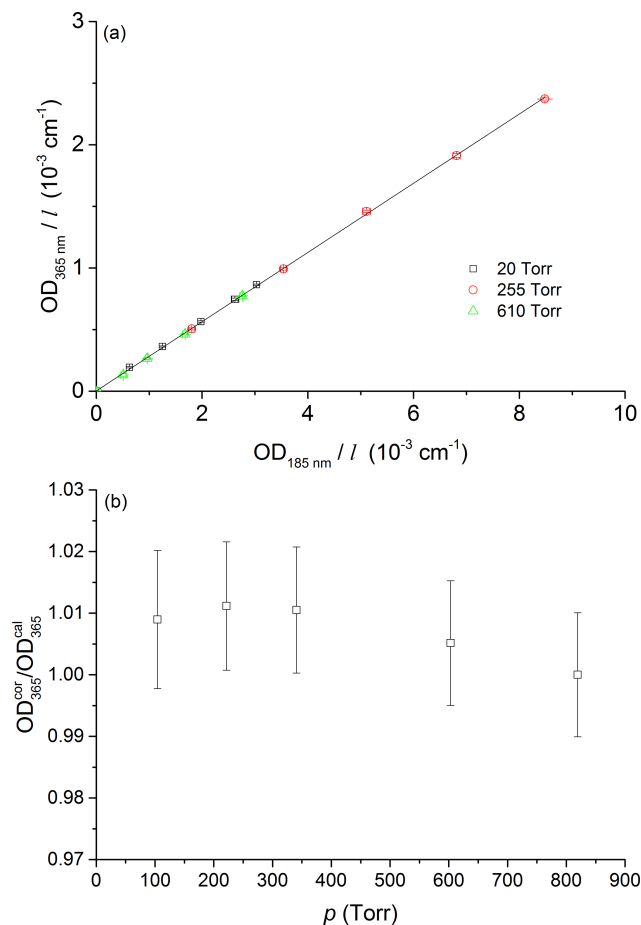
Figure 2. Pressure dependence of the relative NO$_2$ absorption cross section, $\sigma_{365\,nm}/\sigma_{185\,nm}$, at 185 and 365 nm. The solid line is a linear regression for all three datasets giving a slope of 0.281 ± 0.002 (uncertainty is 2σ, statistical only). Panel **(b)** shows the slopes obtained at 20, 255, and 610 Torr plotted versus pressure. The measurements were performed at room temperature.

255, and 610 Torr N$_2$) was recorded simultaneously in the two optical absorption cells. The ODs were corrected for a slight pressure (and thus concentration) difference between the two optical absorption cells and normalized to an optical path length of 1 cm to obtain the parameters OD$_{365}^{cor}$ and OD$_{185}^{cor}$. The linear regression of a plot of OD$_{365}^{cor}$ versus OD$_{185}^{cor}$ yields a value of OD$_{365}^{cor}$/OD$_{185}^{cor}$ = 0.282 ± 0.004 (uncertainty is 2σ) and, within 1 %, is independent of pressure.

In a second set of experiments, the optical density at 365 nm (OD$_{365}$) from 2.1×10^{16} molecule cm^{-3} NO$_2$ in 820 Torr of N$_2$ was initially recorded. The optical absorption cell was then evacuated stepwise to 100 Torr and OD$_{365}$ recorded at each pressure. The NO$_2$ samples contained N$_2$O$_4$ in equilibrium with NO$_2$ (Reactions R8 and R9).

$$NO_2 + NO_2 + M \rightarrow N_2O_4 + M \qquad (R8)$$
$$N_2O_4 + M \rightarrow 2NO_2 + M \qquad (R9)$$
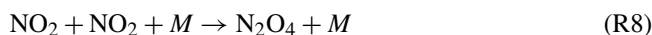
Using the equilibrium coefficient of 2.6×10^{-19} cm^3 molecule^{-1} (average from IUPAC and NASA panels at 298 K) we calculated a N$_2$O$_4$/NO$_2$ ratio that changed from 5.9×10^{-3} at 820 Torr ([NO$_2$] = 2.1×10^{16} molecule cm^{-3}) to 7.0×10^{-4} at 100 Torr (NO$_2$ = 2.56×10^{15} molecule cm^{-3}). OD$_{365}$ was thus corrected ($< 0.3\%$) for the absorption of N$_2$O$_4$ at 365 nm ($\sigma_{365\,nm}$ (N$_2$O$_4$) = 3×10^{-19} cm^2 molecule^{-1}, Burkholder et al., 2015) and for the small change in [NO$_2$] resulting from the shift in equilibrium as the pressure and thus NO$_2$ concentration were reduced. We also corrected for NO$_2$ depletion due to photolysis (to NO and O(^{3}P), $\Phi = 1$) caused by absorption of the 365 nm light. The photolytic loss rate constant of NO$_2$ was determined in a separate experiment to be 8×10^{-6} s^{-1}, which requires a correction in [NO$_2$] of $< 0.2\%$ on the timescale of the experiment. Altogether, the corrections outlined above accounted for less than 2 % of the measured optical density.

In the absence of a pressure dependence of the effective absorption cross section of NO$_2$ at 365 nm, the ratio of measured optical density (OD$_{365}^{cor}$) to that calculated directly (OD$_{365}^{calc}$) from the initial concentration at 820 Torr and the subsequent changes in pressure should not deviate from unity. Figure 2b plots OD$_{365}^{cor}$/OD$_{365}^{cal}$ (normalized to the measurement at 820 Torr) against pressure and indicates that within an experimental uncertainty of 2 %, no pressure dependence in the NO$_2$ absorption cross section at 365 nm is observed.

The two sets of experiments described above show that there is no significant ($< 2\%$) pressure dependence in the effective cross section of NO$_2$ at 365 nm.

3.1.2 Comparison of NO$_2$ literature spectra

The NO$_2$ visible spectra have already been reviewed (Orphal, 2003) and we extend this to include the more recent high-resolution work by Nizkorodov et al. (2004) as it was used as a reference in a recent kinetic study of OH + NO$_2$ (Mollner et al., 2010). At ultra-high resolution, rovibrational lines in the NO$_2$ spectrum broaden at higher pressures and the two more recent studies by Vandaele et al. (2002) and Nizkorodov et al. (2004) reported pressure broadening factors γ (γ being the half width at half maximum of a Lorentzian) in air of 0.081 and 0.116 cm^{-1} atm^{-1} respectively, corresponding to ~ 0.0013 and ~ 0.0019 nm at 1 atm and 405 nm respectively. Using the broadening factors above, one can generate spectra at any pressure by convoluting a pressure-dependent Lorentzian line width to a NO$_2$ spectrum obtained at low pressure and then degrading it (using a Gaussian slit function) to the resolution of the spectrometer. When applying these convolutions to the Vandaele et al. (2002) dataset, we found no difference in cross sections when using their spectra obtained at higher pressure or when using a calculated, pressure-broadened spectrum obtained at low pressure.

We also fitted our experimental measurement of NO$_2$ optical density (405 to 440 nm) using the lower-resolution spectra reported by Merienne et al. (1995) and Yoshino et al. (1997). Use of these reference spectra resulted in excellent agreement with those from Vandaele et al. (2002). This reflects the fact that although line widths increase at increasing pressure, once degraded to our spectral resolution, there is no discernible change in the cross sections in the 410–440 nm range. The same conclusion can be drawn when working with the spectra of Nizkorodov et al. (2004) that were obtained at pressures of < 75 Torr. In contrast, using the NO$_2$ spectra of Nizkorodov et al. (2004), which were recorded at pressures ≥ 75 Torr, resulted in an overestimation of the NO$_2$ concentration by up to 20 % (at 596 Torr) when compared to those listed above. For these reasons, we use the spectrum reported by Vandaele et al. (2002) measured at 80 Torr as a reference spectrum throughout this work. We emphasize that use of any other spectrum (including the Nizkorodov spectrum obtained at low pressure and subsequently broadened (using their parameters) to any other pressure would have no significant impact ($< \sim 3\%$) on the cross section we derived at 365 nm.

### 3.1.3 Effective absorption cross section at 365 nm

The effective cross section of NO$_2$ at 365 nm was determined by measuring its concentration in the 110 cm optical cell using the spectrum of Vandaele et al. (2002) between 400 and 450 nm and simultaneously monitoring the optical density at 365 nm. An example of data used to retrieve the NO$_2$ concentration using the measured optical density (405 to 440 nm) and the spectrum of Vandaele et al. (2002) is given in Fig. 3a.

Figure 3b shows the Beer–Lambert plot used to determine the 365 nm NO$_2$ absorption cross section at room temperature and 190 Torr of N$_2$. The effective cross section derived from the slope is $(5.89 \pm 0.35) \times 10^{-19}$ cm^2 molecule^{-1}. The total uncertainty (6 % at 2σ) takes into account the spread in absorption cross sections (400–450 nm) reported in the literature (Merienne et al., 1995; Yoshino et al., 1997; Vandaele et al., 1998, 2002). Our effective cross section at 365 nm is in excellent agreement with previous values of $(5.75 \pm 0.17) \times 10^{-19}$ cm^2 molecule^{-1} reported by Wine et al. (1979) and D'Ottone et al. (2001), also obtained using low-pressure Hg lamps as emission-line sources.

3.1.4 Detection of NO$_2$ by LIF and NO$_2$ dimerization at low temperatures

At low temperatures and/or high NO$_2$ concentration, NO$_2$ partially dimerizes to N$_2$O$_4$ (Reactions R8 and R9), which will lead to differences in the NO$_2$ concentrations derived from the optical absorption measurements at room temperatures with respect to those in the reactor where the OH + NO$_2$ reaction is investigated. Indeed, at very low temperature, a plot of first-order OH loss constant versus NO$_2$
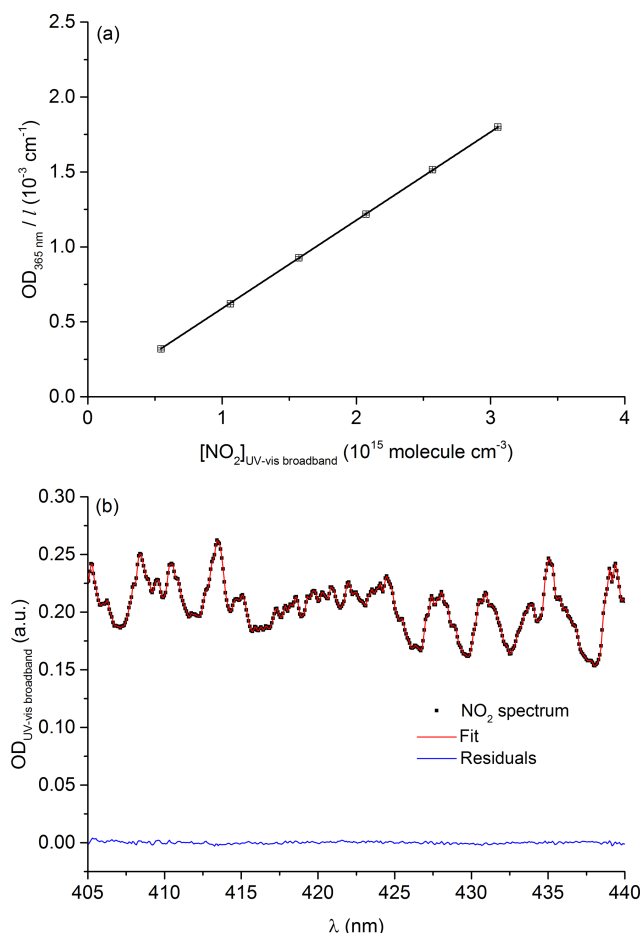
Figure 3. (a) Beer–Lambert plot of $OD_{365\,nm}/l$ as a function of $[NO_2]$ (determined using the long-path UV–vis broadband cell) used to determine the NO$_2$ effective cross section at 365 nm, $\sigma_{365\,nm} = (5.89 \pm 0.24)10^{-19}\,\mathrm{cm}^2$ molecule^{-1}. **(b)** Example of a NO$_2$ spectrum (squares) recorded using the long-path UV–vis broadband cell. The red line shows the fit to the reference spectrum. The blue line is the residual. The experiments were performed at 297 K and 185 Torr.

concentration as measured by optical absorption flattens at high $[NO_2]$ due to the overestimation of the NO$_2$ concentration in the reactor. This is illustrated in Fig. S1 of the Supplement.

The NO$_2$ concentration in the cold reactor may be calculated using the following expression (Brown et al., 1999).

$$[NO_2] = \frac{\left(\sqrt{8[NO_2]_0 K_8 + 1}\right) - 1}{4K_8}, \qquad (2)$$

where $[NO_2]_0$ is the measured concentration in the absorption cells at room temperature and K_8 is the equilibrium constant for Reactions R8 and R9.

At 217 K, K_8 is associated with an uncertainty of $> 50\%$ (Atkinson et al., 2004; Burkholder et al., 2015; IUPAC, 2019) with the value given by IUPAC $\sim 65\%$ smaller than that given by NASA. At 217 K and $[NO_2] = 5\times$

10^{14} molecule cm^{-3}, the different recommendations would lead to a $\sim 13\%$ difference in NO$_2$. Even if K_8 were accurately known, thermal gradients along the length of the reactor and between the walls and the centre of the reactor (where we monitor OH kinetics) could potentially lead to concentration gradients of NO$_2$ and thus to a difference between the concentrations derived from the optical absorption measurements. For these reasons, we checked the validity and the magnitude of the correction that needed to be applied to $[NO_2]$ at low temperatures by performing series of measurements where $[NO_2]$ was measured simultaneously by in situ LIF and UV absorption ($[NO_2]_{UV}$) at different temperatures from 218 to 320 K and constant density (1.65×10^{18} molecule cm^{-3}; corresponding to 50 Torr at 292 K).

Figure 4 displays the NO$_2$ LIF signal at six different temperatures (218, 234, 257, 274, 292, and 320 K) as a function of the NO$_2$ concentration measured by ex situ optical absorption at room temperature. For the three highest temperatures, where N$_2$O$_4$ formation is negligible at the concentrations used, there is a strictly linear dependence of the LIF signal on $[NO_2]$ and no measurable change in the LIF sensitivity with temperature. The latter indicates that any dependence of the LIF efficiency on temperature is very weak. As far as we are aware, none of the previous studies of NO$_2$ fluorescence quenching have reported a temperature dependence of the fluorescence quenching rate constant for N$_2$ (Keil et al., 1980). Only Schurath et al. (1981) report a weak negative T dependence ($T^{-0.42}$) on the fluorescence quenching rate constant for NO$_2$* (formed in the NO + O$_3$ reaction) in N$_2$ between 285 and 446 K, but acknowledge that the T dependence might be erroneous due to the large scatter in their dataset.

The NO$_2$ LIF signals obtained at low temperatures (218 and 234 K) show deviation from linearity as expected if significant amounts of NO$_2$ dimerize to N$_2$O$_4$. In Fig. 4 we plot the expected dependence of the LIF signal from NO$_2$ in the cold reactor on the ex situ NO$_2$ concentration as calculated using Eq. (2) and the equilibrium constant K_8 recommended by IUPAC (solid lines) or NASA (dashed lines). The predicted dependence reproduces the measurements within $\sim 20\%$ confirming that the literature values of equilibrium coefficient are appropriate for correcting NO$_2$ concentrations in kinetic experiments at low temperatures. As our LIF signals at low temperatures lie broadly between those predicted using the equilibrium constants preferred by IUPAC and NASA, we have used an average value of K_8 for correcting NO$_2$ concentrations in the kinetic experiments. We note here that the corrections applied are small and do not impact significantly on the accuracy of the rate coefficient we derive (see later for details).
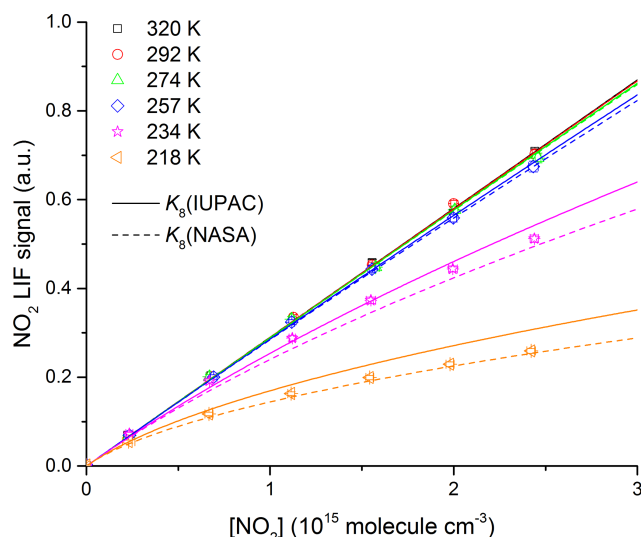
Figure 4. NO$_2$ LIF signal (following excitation at 564 nm) as a function of NO$_2$ concentration at six different temperatures from 218 to 320 K. The experiments were performed in N$_2$ bath gas ([N$_2$] = 1.65×10^{18} molecule cm^{-3}). The lines were derived using the equilibrium constants (K_8) for NO$_2$ dimerization to N$_2$O$_4$ preferred by IUPAC (solid lines) and NASA (dashed lines).

3.2 Rate coefficients for OH + NO$_2$ (k_5)

In this section, we present our measurements of k_5 in N$_2$ and O$_2$ bath gases and compare the results to previous datasets and the parameterizations presently preferred by evaluation panels. The PLP-LIF studies were carried out under pseudo first-order conditions with [NO$_2$] $\gg$ [OH], so that the OH profiles are described by

$$[OH]_t = [OH]_0 \exp(-k't), \qquad (3)$$

where [OH]$_t$ is the concentration (molecule cm^{-3}) at time t after the laser pulse. k' is the pseudo-first-order rate coefficient and is defined as

$$k' = k_5 [NO_2] + k_d, \qquad (4)$$

where k_5 is the bimolecular rate coefficient (cm^3 molecule^{-1} s^{-1}) for the reaction between OH and NO$_2$. k_d (s^{-1}) accounts for OH loss due to diffusion out of the reaction zone and reaction with HNO$_3$ or H$_2$O$_2$. Figures 5 and 6 display representative datasets obtained in N$_2$ bath gas at 295 K and at four different pressures (100, 300, 500, and 900 Torr). OH decays are exponential over > 2 orders of magnitude and the plots of k' versus [NO$_2$] are straight lines as expected from Eq. (4). Values of k_5 derived from these datasets typically have statistical uncertainty (2σ) of less than 5 %.

The overall uncertainty in k_5 is dominated by uncertainty in the NO$_2$ concentration, the origin of which is uncertainty in the NO$_2$ absorption cross sections and in the correction for
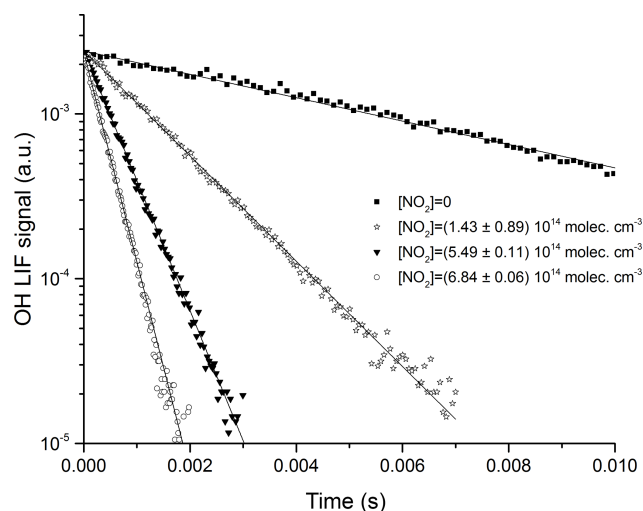
Figure 5. Exponential decay of the OH LIF signal in 100 Torr N$_2$, at 293 K, and at four different NO$_2$ concentrations. OH was generated by the photolysis (at time = 0 s) of H$_2$O$_2$ at 248 nm. The solid lines are fits to the datasets using Eq. (3).
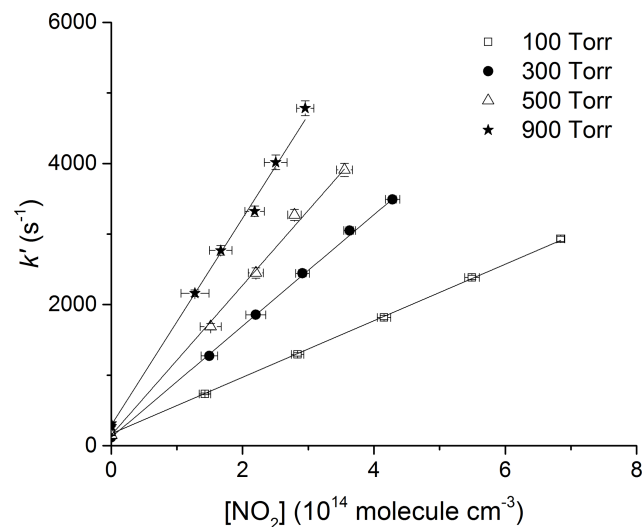
Figure 6. Plots of k' versus [NO$_2$] at four different pressures in N$_2$ and at 295 K. The lines are least-squares fits to the data using Eq. (4). Error bars are 2σ statistical only.

NO$_2$ dimerization to N$_2$O$_4$. The NO$_2$ concentration used to determine the rate coefficient was the average of those determined by analysing the optical density between 405 and 450 nm in the 110 cm absorption cell located upstream of the reactor and the optical density at 365 nm measured in the 43.8 nm optical absorption cell located downstream of the reactor. The two concentrations generally agreed to better than 2 %. The optical absorption measurements of NO$_2$ were made at room temperature. However, when the reactor is operated at low temperatures some NO$_2$ is converted to N$_2$O$_4$ via the equilibrium (R8) and a correction must be

made to account for the difference in $[NO_2]$ between the optical absorption measurement and that present in the reactor (see Sect. 3.1.4). At temperatures above 273 K, no correction to $[NO_2]$ was necessary, but amounted to 0.5 % to 3.5 % at 245 K, 4 % to 26 % at 229 K and 6 % to 29 % at 217 K, with the largest corrections being associated with the highest NO_2 concentrations. The total uncertainty associated with each value of k_5 is listed in Table 1 and considers uncertainty in NO_2 concentration measurement (i.e. uncertainty associated with NO_2 cross sections and the equilibrium constant for NO_2 dimerization) as well as statistical error on the fits to derive k' (Fig. 6). The expression used to calculate the total overall uncertainty for each value of k_5 is given in the Supplement and results in ~ 8 % at $T > 240$ K and ~ 16 % for measurements at 217 and 229 K.

Apart from the use of different OH precursors (values of k_5 derived when using photolysis of either H_2O_2 or HNO_3 were not significantly different), experiments were carried out to investigate the effect of different initial OH concentrations. In two sets of experiments, at total pressures of either 200 or 500 Torr N_2, the 248 nm laser fluence was varied by a factor of 7 (from ~ 5 to 35 mJ cm^{-2}) and the H_2O_2 and HNO_3 concentrations by 4 and 6 respectively, resulting (at 200 Torr) in a factor of 10 change in $[OH]_0$ (from $\sim 10^{11}$ to 10^{12} molecule cm^{-3}) (see Table 1). Reducing the laser repetition rate from 10 to 5 Hz had no discernible effect on the value of k_5 retrieved ($10.6 \pm 0.6 \times 10^{-12}$ cm^3 molecule^{-1} s^{-1} at 10 Hz and $10.7 \pm 0.1 \times 10^{-12}$ cm^3 molecule^{-1} s^{-1} at 5 Hz; see Table 1, rate coefficients at 293 K and 498.5 Torr).

The results indicate that, within the range of OH mentioned above, there is no significant influence of secondary reactions of OH on the determination of k_5. For the $OH + NO_2$ reaction, the use of OH concentrations as high as 10^{12} molecule cm^{-3} is not expected to have a significant impact on the OH decay rates because the major product, HNO_3, reacts only slowly with OH, with $k(OH + HNO_3) = 1.6 \times 10^{-13}$ cm^3 molecule^{-1} s^{-1} at 296 K and 250 Torr (Dulitz et al., 2018). Even if the minor product, HOONO, were to react with OH with a rate coefficient of 2×10^{-10} cm^3 molecule^{-1} s^{-1} (i.e. close to collision frequency), this would still have an impact of less than 2 % on the first-order OH decay rate coefficient at 750 Torr pressure.

The self-reaction of OH at an initial concentration of 1×10^{12} molecule cm^{-3} results in a loss rate of ~ 15 s^{-1}, which is negligible compared to typical decay constants of ~ 1000 to $10\,000$ s^{-1} due to reaction with NO_2. Photolysis of NO_2 is inefficient as the cross section of NO_2 is low at 248 nm (1×10^{-20} cm^2 molecule^{-1}; IUPAC, 2019) but can result in approximately equivalent initial O(^{3}P) and OH concentrations. However, the presence of O(^{3}P) has a negligible impact as its fate is mainly reaction with NO_2 to form NO, which also reacts only slowly with OH.

**Table 1.** Measurements of k_5 in N_2 and O_2 bath gases.

p^a	T^b	M^c	OH precursor	$[OH]_0^d$	k_5^e	$[NO_2]$ correction^f
N_2 bath gas						
22.4		1.00	HNO_3	1.8	3.78 ± 0.76	12–24
39.7	217	1.77	HNO_3	1.4	5.50 ± 1.18	6–22
56.2		2.50	HNO_3	1.0	6.99 ± 0.99	8–16
78.8		3.51	HNO_3	1.0	8.70 ± 1.59	6–29
12.3		0.52	HNO_3	2.3	1.84 ± 0.43	12–26
18.5		0.78	HNO_3	3.7	2.62 ± 0.39	6–14
38.5	229	1.62	HNO_3	3.8	4.82 ± 0.91	8–18
79.5		3.35	HNO_3	2.7	7.63 ± 0.79	4–14
117.1		4.94	HNO_3	4.2	9.18 ± 1.10	8–18
158.8		6.66	HNO_3	5.4	11.0 ± 1.23	4–13
22.4		0.88	HNO_3	1.1	2.75 ± 0.19	0.5–3.5
44.9		1.77	HNO_3	2.2	4.47 ± 0.32	0.9–2.8
63.7	245	2.51	HNO_3	2.2	5.41 ± 0.37	0.5–3.2
84.4		3.33	HNO_3	1.8	6.39 ± 0.45	0.5–3.5
122.8		4.84	HNO_3	1.5	8.01 ± 0.72	0.8–2.5
165		6.50	HNO_3	2.7	9.60 ± 0.82	0.9–2.8
100.4	273	3.53	H_2O_2	8.7	5.07 ± 0.36	0
12.3		0.41	HNO_3	5.5	0.96 ± 0.07	0
13.3		0.44	H_2O_2	2.5	0.98 ± 0.16	0
20.1		0.66	H_2O_2	3.4	1.34 ± 0.09	0
25.5		0.84	H_2O_2	1.9	1.66 ± 0.12	0
26.4		0.87	H_2O_2	13.3	1.65 ± 0.12	0
36.8		1.22	H_2O_2	2.3	2.11 ± 0.13	0
50.2		1.65	H_2O_2	6.2	2.58 ± 0.16	0
56.8		1.88	H_2O_2	3.7	2.88 ± 0.19	0
75.6		2.50	H_2O_2	2.0	3.41 ± 0.21	0
99.3		3.25	H_2O_2	5.8	3.90 ± 0.35	0
99.9		3.28	H_2O_2	5.2	4.05 ± 0.25	0
102.3		3.37	HNO_3	14.3	4.14 ± 0.29	0
131.6		4.35	H_2O_2	1.7	4.98 ± 0.33	0
133.3		4.41	H_2O_2	1.6	5.07 ± 0.36	0
160.5		5.31	H_2O_2	1.6	5.69 ± 0.40	0
199.8		6.52	H_2O_2	4.6	6.19 ± 0.52	0
199.9	293	6.56	HNO_3	11.3	6.12 ± 0.42	0
200.8		6.59	HNO_3	1.1	6.69 ± 0.49	0
250.4		8.27	H_2O_2	3.4	7.26 ± 0.46	0
299.4		9.82	HNO_3	10.7	7.80 ± 0.55	0
299.5		9.82	H_2O_2	3.9	8.02 ± 0.55	0
299.5		9.81	HNO_3	11.7	8.43 ± 1.18	0
401		13.20	HNO_3	11.2	9.23 ± 0.86	0
401.3		13.20	H_2O_2	3.8	9.71 ± 0.84	0
498.5		16.30	H_2O_2	7.3	10.6 ± 0.87	0
498.5		16.30	H_2O_2	7.6	10.7 ± 0.66^g	0
498.7		16.40	HNO_3	15.3	11.1 ± 0.72	0
498.8		16.40	H_2O_2	4.5	11.0 ± 0.73	0
598.8		19.70	H_2O_2	5.1	11.4 ± 1.09	0
603.1		19.80	HNO_3	15.9	12.2 ± 0.76	0
705.5		23.20	H_2O_2	4.9	13.6 ± 1.36	0
709.6		23.30	HNO_3	11.6	12.9 ± 1.10	0
796.7		26.20	H_2O_2	10.0	13.3 ± 1.11	0
901.1		29.50	H_2O_2	10.3	14.8 ± 1.34	0
115.6		3.35	H_2O_2	9.9	2.91 ± 0.21	0
342.3	333	9.93	H_2O_2	4.5	6.67 ± 0.48	0
569.9		16.52	H_2O_2	5.2	8.88 ± 0.82	0
794.6		23.04	H_2O_2	5.1	10.15 ± 1.13	0

Table 1. Continued.

p^a	T^b	M^c	OH precursor	$[OH]_0^d$	k_5^e	$[NO_2]$ correction^f
O$_2$ bath gas						
99.2		3.25	H$_2$O$_2$	24.5	3.31 ± 0.29	0
50.2		1.64	H$_2$O$_2$	13.7	2.16 ± 0.16	0
202.3	293	6.64	H$_2$O$_2$	25.7	5.47 ± 0.43	0
150.7		4.94	H$_2$O$_2$	17.9	4.50 ± 0.33	0
250.6		8.22	H$_2$O$_2$	18.1	6.03 ± 0.39	0

^{a} In torr. ^{b} In kelvin. ^{c} In 10^{18} molecules per cubic centimetre. ^{d} In 10^{11} molecules per cubic centimetre, the OH concentration was calculated from the 248 nm laser fluence, H$_2$O$_2$ or HNO$_3$ concentrations and the respective quantum yield for OH production. ^{e} In 10^{-12} cubic centimetres per molecule per second (errors are total uncertainty, 2σ). ^{f} As a percentage; due to dimerization of NO$_2$ to N$_2$O$_4$, which is insignificant at temperatures > 273 K. ^{g} Experiment performed at a laser repetition rate of 5 Hz (instead of the usual 10 Hz).
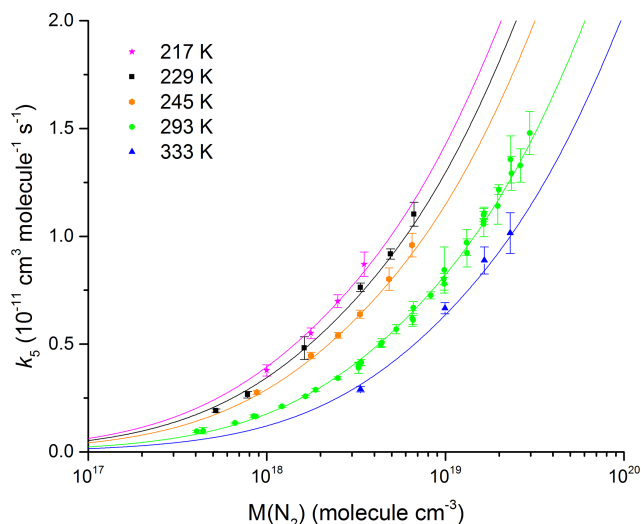
Figure 7. Rate coefficient, k_5, as a function of N$_2$ density in the fall-off range for five different temperatures. The error bars represent 2σ statistical uncertainty. The solid line fits to the data are described by Eq. (5) with $k_0 = 2.6 \times 10^{-30}$ cm^6 molecule^{-2} s^{-1}, $m = 3.6$, $n = 0$, $k_\infty = 6.3 \times 10^{-11}$ cm^3 molecule^{-1} s^{-1}, and $F_c = 0.39$ (fixed).

3.2.1 Measurements of k_5 in N$_2$ bath gas and comparison with literature

Our measurements of k_5 in N$_2$ bath gas (12–900 Torr, 217–333 K) are summarized in Fig. 7 and listed in Table 1.

The solid lines in Fig. 7 are fits according to the Troe formalism for termolecular reactions (Troe, 1983) as adopted by the IUPAC panel:

$$k_5(p, T) = \frac{\beta k_0 \left(\frac{T}{300}\right)^{-m} M k_\infty \left(\frac{T}{300}\right)^{-n}}{\beta k_0 \left(\frac{T}{300}\right)^{-m} M + k_\infty \left(\frac{T}{300}\right)^{-n}} \log F, \tag{5}$$

where k_0 is the low-pressure limit rate coefficient in cm^6 molecule^{-2} s^{-1}, k_∞ is the high-pressure limit rate coefficient in cm^3 molecule^{-1} s^{-1}, T is the temperature in kelvin, M is the density in molecules per cubic metre, and m and n are dimensionless temperature exponents. β takes into ac-

count the overall collision efficiency for energy transfer from the initially formed OH–NO$_2$ association complex to the bath gases, with

$$\beta = \sum \beta_i x_i, \tag{6}$$

where β_i and x_i are the collision efficiency and the mixing ratio of bath gas i respectively.

The broadening factor, F, is defined as

$$\log F = \frac{\log F_c}{1 + \left[\log\left(\frac{\beta k_0 \left(\frac{T}{300}\right)^{-m} M}{k_\infty \left(\frac{T}{300}\right)^{-n}}\right)/N\right]^2}, \tag{7}$$

where $N = [0.75 - 1.27 \log F_c]$ and F_c is the broadening factor at the centre of the fall-off curve.

Accurate representation of termolecular rate coefficients using this expression requires data on the low- and high-pressure limiting rate coefficients, k_0 and k_∞, and their temperature dependence. Data close to the low-pressure limit have generally been obtained using low-pressure flow tubes (Howard, 1979; Keyser, 1984), whereas measurements close to the high-pressure limit required equipment capable of operation at several hundred bar or the use of a different approach in which the rate coefficient for relaxation of vibrationally excited OH in collision with NO$_2$ is equated to the high-pressure limit of the association reaction.

In the case of the title reaction, several measurements have been performed close to the low-pressure limit (0.5 to 10 Torr) (Anderson and Kaufman, 1972; Anderson et al., 1974; Anderson, 1980; Burrows et al., 1983; Howard and Evenson, 1974), while only one group has carried out experiments at pressures approaching the high-pressure limit (Hippler et al., 2002, 2006). Even at 500 bar He, the reaction of OH with NO$_2$ is still not at the high-pressure limit, and at pressures as low as 10 Torr of He, there is already evidence for significant fall-off. The two determinations (D'Ottone et al., 2005; Smith and Williams, 1985) of the rate constant for vibrational relaxation of OH in collision with NO$_2$ deviate in their value of k_∞ by ~ 25 %. For many termolecular reactions, limitations in data quality mean that k_0 or k_∞ is often derived by fitting to multiple datasets that span a large range of pressures and fixing F_c to either a theoretical value (IUPAC, 2019) or to a value of 0.6 (Burkholder et al., 2015). To analyse our data we used a similar approach to that of IUPAC with the broadening factor fixed to 0.39 (Cobos and Troe, 2003). In order to further reduce the number of variables when fitting data to expression (Eq. 7) we also make the assumption that k_∞ is independent of temperature ($n = 0$). This assumption is reasonable as the value of n is expected to be much smaller than that of m and the data at high pressures are not of sufficient quality to constrain this parameter.

By fitting our data (217, 229, 245, 273, 293, and 333 K) to expression (Eq. 7) and allowing k_0, m, and k_∞ to vary, we derive values of $k_0 = 2.6 \times 10^{-30}$ cm^6 molecule^{-2} s^{-1},

$k_\infty = 6.3 \times 10^{-11}$ cm^3 molecule^{-1} s^{-1}, and $m = 3.6$. These parameters accurately reproduce the pressure and temperature dependence of k_5, which we observe in N$_2$ bath gas (see Fig. 7) with most of the individual rate coefficients measured agreeing to better than 5 % of the parametrization. This is highlighted in Fig. S2, which shows the percentage deviation of each data point from the value derived using the values of k_0, k_∞, n, m, and F_c listed above.

We now compare our value of k_0 to those reported from low-pressure flow-tube studies of the title reaction. We note that, in low-pressure flow tubes operated at pressures greater than a few torr of N$_2$, mixing effects and OH losses to walls severely impede accurate kinetic measurements of OH rate coefficients, especially at low temperatures (Brown, 1978; Howard, 1979). In their study of the reaction between OH and NO$_2$, Howard and Evenson (1974) do not report rate coefficients at pressures greater than 2 Torr N$_2$ because of the large uncertainty resulting from the corrections applied. In low-pressure flow-tube studies of the OH + NO$_2$ reaction, the loss rate constant for OH (k') is a composite term (Eq. 8), with contributions from the association reaction ($k_5[\text{NO}_2]$, slow at low pressures), the loss of OH to the bare flow-tube wall (k_w, experimentally derived in the absence of NO$_2$), and the heterogeneous loss of OH due to reaction with surface-adsorbed NO$_2$ ($k_s[\text{NO}_2]_s$), which depends on the rate coefficient for the surface reaction (k_s) and the availability of surface-adsorbed NO$_2$ ([NO$_2$]$_s$), with the latter dependent in a non-linear manner (via a gas-surface partition coefficient) on the gas-phase NO$_2$ concentration.

$$k' = k_5\,[\text{NO}_2] + k_w + k_s[\text{NO}_2]_s \qquad (8)$$

In low-pressure flow-tube studies, correction is rarely made for the surface-reaction-induced heterogeneous loss of OH, in this case $k_s[\text{NO}_2]_s$, the manifestation of which is often a positive intercept in plots of k_{bi} as a function of molecular density (Anderson et al., 1974; Howard and Evenson, 1974).

For the reaction of OH + NO$_2$ in N$_2$, low-pressure flow-tube studies report values of k_0 between 2.0 and 2.9×10^{-30} cm^6 molecule^{-2} s^{-1} close to room temperature. Although this range is consistent with the value we derive (2.6×10^{-30} cm^6 molecule^{-2} s^{-1}), the agreement is to some extent fortuitous for reasons outlined above and also because the low-pressure flow-tube studies of the reaction between OH and NO$_2$ report values of k_0 that were derived by assuming a linear dependence of the rate coefficient on pressure. Our precise dataset and the parameterization with broad fall-off behaviour indicate significant deviation from linear behaviour at pressures of 2 Torr of N$_2$. In order to estimate the size of the error made by assuming linear behaviour, we calculated rate coefficients for the pressure range of 0.5 to 10 Torr of N$_2$ using fall-off curves with $F_c = 0.39$, $k_0 = 2.6 \times 10^{-30}$ cm^6 molecule^{-2} s^{-1} and $k_\infty = 6.3 \times 10^{-11}$ cm^3 molecule^{-1} s^{-1}. Unweighted linear fitting of the rate coefficients thus obtained resulted in
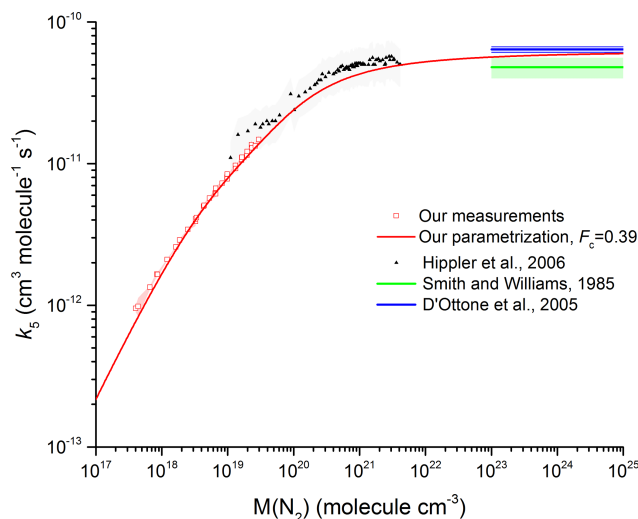
Figure 8. Comparison between our results in N$_2$ with the measurements by Hippler et al. (2006) (He bath gas; the grey shaded area represents total uncertainty) and the high-pressure limits derived by Smith and Williams (1985) and D'Ottone et al. (2005). All measurements are close to 298 K. The red line was obtained using Eq. (5) with $k_0 = 2.6 \times 10^{-30}$ cm^6 molecule^{-2} s^{-1}, $m = 3.6$, $n = 0$, $k_\infty = 6.3 \times 10^{-11}$ cm^3 molecule^{-1} s^{-1}, and $F_c = 0.39$ (fixed).

a value of $k_0 = 2.3 \times 10^{-30}$ cm^6 molecule^{-2} s^{-1}, an underestimation of 15 % (when fitted up to 2 Torr), which increases to 25 % when the fit is extended to 10 Torr. The values of k_0 obtained in the low-pressure flow-tube studies are thus likely to be biased to lower values, especially those that extend to pressures above 2 Torr N$_2$, though the effects of fall-off may not be evident in the highly scattered original datasets. The two low-pressure flow-tube studies (Anderson, 1980; Howard and Evenson, 1974) (both up to 2 Torr N$_2$) that reported rate coefficients at various pressures and the value of k_0 derived are compared to our parameterization in Fig. S3. The data of Anderson (1980) are limited in number and display large scatter. The reported value (at 300 K) of $k_0 = 2.3 \times 10^{-30}$ cm^6 molecule^{-2} s^{-1} appears to have been obtained from a linear fit with the intercept fixed to zero. The original rate coefficients by Howard and Evenson (1974) display better precision, but indicate a large intercept at zero pressure of 1.8×10^{-14} cm^3 molecule^{-1} s^{-1}. The data simply corrected by subtracting a pressure-independent offset still lie ~ 20 % above our parametrization. We conclude that the low-pressure flow-tube studies of the rate coefficient for OH + NO$_2$ are not of sufficient precision or accuracy to define k_0 for the purpose of obtaining an accurate parameterization of the rate coefficient, k_5.

We now compare our value of k_∞ (6.3×10^{-11} cm^3 molecule^{-1} s^{-1}) to literature values. Figure 8 shows our data at 293 K (open symbols) along with values of k_∞ (blue- and green-shaded areas) derived from the vibrational relaxation of OH (D'Ottone et al., 2005;

Smith and Williams, 1985). The height of the shaded areas indicates the reported overall uncertainty. We also plot the rate coefficients of Hippler et al. (2006) obtained at high pressure in He. To compare our measurements in N_2 with the high-pressure data in He, we scaled the He pressure by a factor of 0.39 (determined in our laboratory). We recognize that this is not a rigorous treatment of the relative collision efficiency of N_2 and He data close to the high-pressure limit, but note that using a more complex approach (i.e. using a density-dependent correction and bath-gas-dependent values of F_c) would lead to only insignificant changes in the equivalent N_2 pressure. The solid red line is our parameterization with the values of k_0, k_∞, and F_c given above and is seen to reproduce the trend in k_5 with pressure between 16 mbar and 190 bar N_2. Our value for k_∞ of $(6.3 \pm 0.4) \times 10^{-11}$ cm^3 molecule^{-1} s^{-1} (error given at 2σ statistical only) is consistent within combined uncertainty with those of $(6.4 \pm 0.3) \times 10^{-11}$ cm^3 molecule^{-1} s^{-1} obtained by D'Ottone et al. (2005) and $(4.8 \pm 0.8) \times 10^{-11}$ cm^3 molecule^{-1} s^{-1} obtained by Smith and Williams (1985).

In this section, we compare our values of k_0 and k_∞ to those obtained in previous experiments at pressures in the fall-off regime, in which OH was generated photolytically. First, we note that values of k_0 and k_∞ and m obtained by fitting pressure-dependent datasets are strongly dependent on the choice of F_c and (to a lesser extent) whether an asymmetric (IUPAC) or symmetric (NASA) broadening factor has been used. In order to make a meaningful comparison between our values of k_0, k_∞, and m and those previously reported in the literature, we have therefore re-fitted the existing datasets using Eq. (5) with F_c fixed to 0.39. The results, presented in Table 2, show a variation of larger than a factor of 2 for both k_0 (1.8 to 3.8×10^{-30} cm^6 molecule^{-2} s^{-1}) and k_∞ (3.4 to 7.9×10^{-11} cm^3 molecule^{-1} s^{-1}) even though similar experimental procedures were used. Our value of 3.60 for m (describing the temperature dependence of k_0) is lower than those obtained from re-analysis of the datasets of Anastasi and Smith (1976), Wine et al. (1979), and Brown et al. (1999), which lie between 4.5 and 4.9. When the extensive dataset of Brown et al. (1999) is examined more closely, we find that excluding their room temperature data (the discrepancy at room temperature between our two works is discussed below) and only fit their four lowest temperatures (from 220 to 250 K) we would obtain a m of 3.9, in agreement with our dataset. We note that the IUPAC and NASA evaluation panels recommend different values for m. While IUPAC have $m = 4.5$ for both reaction channels, NASA suggest use of 3 and 3.9 for HNO₃ and HOONO forming Reaction R5a and R5b respectively.

In a series of figures (Figs. S4–S10), we compare values of k_5 derived from our parameterization with those presented in previous studies of k_5 in N_2 bath gas over a similar pressure range. There are five previous flash/laser photolysis studies of the title reaction in N_2 bath gas (Anastasi and

Table 2. Re-analysis of previous datasets using $F_c = 0.39$.

	$k_0^{a,b}$	m^a	$k_\infty^{a,c}$	p (Torr)	T (K)
This work	2.6	3.6	6.3	12–900	217–333
Anastasi and Smith (1976)	3.4	4.7	3.4	10–500	220–550
Wine et al. (1979)	3.0	4.9	3.6	15–200	247–352
Brown et al. (1999)	2.3	4.5	4.8	20–250	220–296
D'Ottone et al. (2001)	3.8	0.3	3.8	30–700	273–298
Hippler et al. (2006)	2.5	–	7.3	600–147 000	298
Mollner et al. (2010)	1.8		7.9	50–900	298

^{a} Values listed may deviate from those previously reported owing to use of $F_c = 0.39$ to re-analyse data. ^{b} Units are 10^{-30} cm^6 molecule^{-2} s^{-1}. ^{c} Units are 10^{-11} cm^3 molecule^{-1} s^{-1}.

Smith, 1976; Brown et al., 1999; D'Ottone et al., 2001; Mollner et al., 2010; Wine et al., 1979). Three of these studies (Brown et al., 1999; D'Ottone et al., 2001; Wine et al., 1979) measured NO₂ concentrations in situ at 365 nm using a cross section that deviated by less than 3 % from that reported in the present study (see Sect. 3.1.3).

Anastasi and Smith (1976) reported values of k_5 (Fig. S4) over a wide range of temperatures (220 to 550 K) and pressures (10 to 500 Torr) using flash photolysis of H_2O or HNO₃ as OH precursor with the detection of OH by resonance absorption. The NO₂ concentration was obtained manometrically and no details pertaining to corrections for NO₂ dimerization at low temperatures were given. Our parametrization reproduces most of their data within their experimental uncertainty (reported to be 36 % at 2σ).

Wine et al. (1979) reported temperature-dependent values of k_5 (Fig. S5) in a more limited pressure range (up to $\sim$ 200 Torr in N_2) using laser photolysis of HNO₃ to generate OH and resonance fluorescence to detect it. Our parameterization is in good agreement (better than 10 %) with most of their data apart from at higher pressures points where the difference is > 30 % and greater than the combined quoted uncertainties.

Figure S6 compares our parameterization to the data of Brown et al. (1999) whose methods (PLP-LIF) were very similar to the present study. Their data are however limited to pressures of less than 250 Torr N_2. At molecular densities of less than $\sim$ 7 $\times$ 10^{18} molecule cm^{-3} there is good agreement (< 10 % deviation) but this increases to $\sim$ 20 % at their highest pressures ($M = 1 \times 10^{19}$ molecule cm^{-3}) and is largest at room temperature where it increases to 40 %. Compared to the present study, Brown et al. (1999) worked at lower concentrations of NO₂ (< 2 $\times$ 10^{14} molecule cm^{-3}) in order to limit the formation of N_2O_4 at low temperatures. N_2O_4 formation is however not significant at 298 K and cannot explain the poor agreement at this temperature.

The dataset of D'Ottone et al. (2001) was also obtained using PLP-LIF and also covered a similar range of pressures (100 to 700 Torr N_2 at 298 and 273 K) to the present study. At room temperature, most of their measurements agree within 10 % with our parameterization (Fig. S7); however their values for k_5 obtained at 273 K are consistently

lower by $\sim 25\,\%$. In fact, their measurements at 273 and 298 K are indistinguishable and thus do not display the temperature dependence observed by all previous studies

The most recent dataset (Mollner et al., 2010) was also obtained using PLP-LIF and covered pressures up to 900 Torr N₂ at 298 K. Mollner et al. (2010) monitored NO₂ in situ via UV–visible broadband absorption using reference spectra from Vandaele et al. (2002) and Nizkorodov et al. (2004), though it is not clear how these two spectra were used or combined.

In Sect. 3.1.2, we indicated that using the spectra of Nizkorodov et al. (2004) that were obtained at pressures > 75 Torr could lead to an overestimation of the NO₂ concentration, which would result in an underestimation of k_5. We are unable to assess the extent to which this may have influenced the Mollner et al. (2010) values of k_5. On average, our parametrization overestimates their measurement of k_5 by $\sim 15\,\%$ (Fig. S8).

Values of k_5 in the fall-off regime have also been obtained using a high-pressure laminar flow-tube set up (Donahue et al., 1997; Dransfield et al., 1999) with OH detection by LIF and NO₂ concentrations derived by recording the concentration of a passive tracer (CF₂Cl₂) using FTIR and UV absorption in mixtures of NO₂ and CF₂Cl₂. Figures S9 and S10 indicate poor agreement between this dataset and our parameterization, the disagreement being most significant (factor 2) at room temperature. The discrepancy is smaller at low temperature with our parametrization predicting rates $\sim 5\,\%$ to 25 % faster in the 212.5 and 265 K temperature range.

The comparison of the various datasets reveals differences in the rate coefficients measured in N₂ that cannot be easily explained. All studies worked under pseudo-first-order conditions. Any discrepancy in k_5 between two independent studies is most likely related to the accuracy with which the concentration of NO₂ was measured, with secondary chemistry or reaction of OH with impurities unlikely to be important for reasons already discussed. The PLP-LIF studies used online measurement of NO₂ with almost identical absorption cross sections at 365 nm, or NO₂ reference spectra with absorption cross sections that agree to within a few percent (more details in Sect. 3.1.2). In our work, we recorded the NO₂ concentration using both methods (i.e. 365 nm and UV broadband absorption) and found no evidence for systematic bias in the NO₂ concentration. Also, we showed that the NO₂ cross sections are not influenced significantly by pressure. We have not identified the origin of discrepancies between these datasets but note that the plots of k_5 versus pressure in the present study are generally less scattered than in most other studies, and thus provide better constraint when deriving values for k_0 and k_∞ (Figs. 7, 10, S4–S8).

In Fig. 9, we compare our parametrization to those of IUPAC and NASA at four different temperatures in N₂. At pressures close to 1 bar and 300 K ($M \sim 2.4 \times 10^{19}$ molecule cm⁻³), the IUPAC parameterization underpredicts k_5 slightly ($k_5^{\text{this work}}/k_5^{\text{IUPAC}} \sim 1.11$)
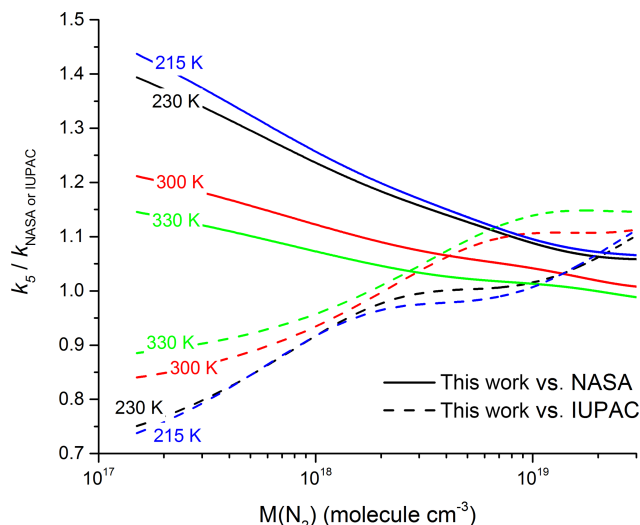

Figure 9. Ratio of our parametrized rate coefficient k_5 versus those calculated from the parameters recommended by IUPAC (dashed lines) and NASA (solid lines) for four different temperatures.

whereas the NASA parameterization is in good agreement ($k_5^{\text{this work}}/k_5^{\text{NASA}} \sim 1.01$). At molecular densities and temperatures typical of the mid-latitude upper troposphere of 230 K and $M = 8 \times 10^{18}$ molecule cm⁻³ (~ 250 mbar) the situation reverses with IUPAC accurately predicting our measured values ($k_5^{\text{this work}}/k_5^{\text{IUPAC}} \sim 1.00$) and NASA overpredicting slightly ($k_5^{\text{this work}}/k_5^{\text{NASA}} \sim 1.10$). As we move up to higher altitudes the discrepancy between measurement and the NASA recommendation increases: taking a typical value of $M \sim 2 \times 10^{18}$ molecule cm⁻³ for the lower stratosphere (20 km altitude) and a temperature of 215 K, we calculate ($k_5^{\text{this work}}/k_5^{\text{IUPAC}} \sim 0.95$) and ($k_5^{\text{this work}}/k_5^{\text{NASA}} \sim 1.20$). Moving up to 35 km altitude ($M \sim 2 \times 10^{17}$ molecule cm⁻³, $T = 230$ K) deviation becomes substantial for both sets of recommendations with ($k_5^{\text{this work}}/k_5^{\text{IUPAC}} \sim 0.75$) and ($k_5^{\text{this work}}/k_5^{\text{NASA}} \sim 1.35$).

The great discrepancy between the IUPAC and NASA recommendations at low pressures and temperatures has its origin in the treatment of the low-pressure limit rate coefficient, k_0. In the IUPAC approach, the parametrization was constrained to the low-pressure datasets (Troe, 2012), extrapolating reported values of k_0 to a higher value assuming the data were in a pure third-order regime; however, as shown above this assumption results in an overestimation of k_0. By fixing F_c to 0.6 and constraining the fit to the high-pressure measurements of Hippler et al. (2006), the NASA parametrization will tend to underestimate k_0.

In order to test this, we fitted our data to the expression used by NASA (Eq. 9) with F_c fixed at 0.6. This resulted in values of $k_0(\text{N}_2) = 2.0 \times 10^{-30}$ cm⁶ molecule⁻² s⁻¹ and $k_\infty = 3.6 \times 10^{-11}$ cm³ molecule⁻¹ s⁻¹ (m stayed unchanged with a fitted value of 3.6), which are not consistent with ei-
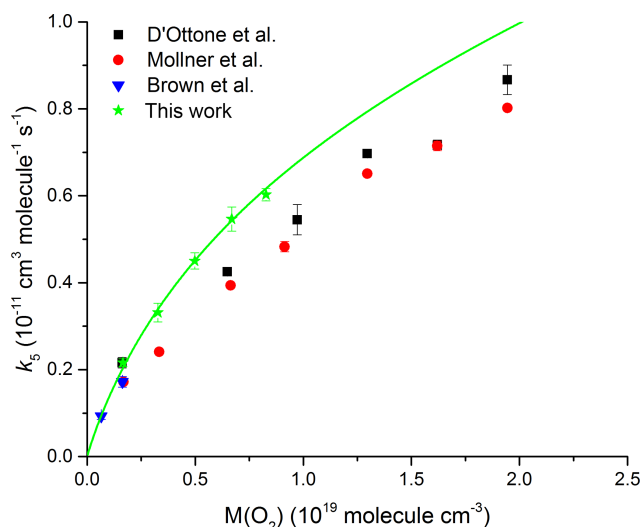
Figure 10. Rate coefficient k_5 as a function of O$_2$ density at $T = 293$ K. The green data points are from the present study; the solid line represents a fit using Eq. (5) with $k_0 = 2.0 \times 10^{-30}$ cm^6 molecule^{-2} s^{-1}, $k_\infty = 6.3 \times 10^{-11}$ cm^3 molecule^{-1} s^{-1} (fixed), $F_c = 0.39$ (fixed), and $m = 3.6$ (fixed).

ther the high- or low-pressure data.

$$k_{\text{NASA}}(p, T) = \frac{k_0 \left(\frac{T}{300}\right)^{-m} M}{1 + \frac{k_0 \left(\frac{T}{300}\right)^{-m} M}{k_\infty \left(\frac{T}{300}\right)^{-n}}} 0.6^{\left\{1 + \left[\log\left(\frac{k_0 \left(\frac{T}{300}\right)^{-m} M}{k_\infty \left(\frac{T}{300}\right)^{-n}}\right)\right]^2\right\}^{-1}} \quad (9)$$

3.2.2 Measurements of k_5 in O$_2$ bath gas and comparison with literature

Brown et al. (1999) were the first to recognize that the third-body collision efficiency of O$_2$ was lower than N$_2$ and, as a consequence, k_5 would be lower in air than in pure N$_2$. This was confirmed in subsequent measurements by D'Ottone et al. (2001) and Mollner et al. (2010).

We have also performed a series of measurements, displayed in Fig. 10, in pure O$_2$ bath gas (50–250 Torr, 295 K). The solid line is a fit to the data using expression (Eq. 5) whereby only k_0 was varied with k_∞, F_c, and m fixed as 6.3×10^{-11} cm^3 molecule^{-1} s^{-1}, 0.39, and 3.6 respectively. The rate coefficients obtained in pure O$_2$ bath gas are in good agreement with the single low-pressure data point of Brown et al. (1999) but are systematically higher (by on average 10 % and 30 % respectively) than those reported by D'Ottone et al. (2001) and Mollner et al. (2010). As for the experiments in N$_2$, the reason for this discrepancy is not obvious.

Our analysis results in a low-pressure limit of $k_0(O_2) = 2.0 \times 10^{-30}$ cm^6 molecule^{-2} s^{-1} and thus a relative collision efficiency of 0.74 for O$_2$ compared to N$_2$. This result is in excellent agreement with the results by Brown et al. (1999) (0.70), D'Ottone et al. (2001) (0.67),

and Mollner et al. (2010) (0.67) and results in a collision efficiency in air (~ 80 % N$_2$ and ~ 20 % O$_2$) of 0.94 relative to N$_2$. The impact of the lower efficiency for collisional deactivation of O$_2$ compared to N$_2$ will be largest close to the low-pressure limit and tends to zero as we approach the high-pressure limit. At low pressures, we calculate a rate coefficient that will be lower by 5 % in air compared to N$_2$, while at 1 atm, the reduction in k_5 will be ~ 3 %. To date, the NASA evaluation panel has incorporated this effect into its recommendations, whereas the IUPAC panel has not. We have not investigated the temperature dependence of the low-pressure rate coefficient (m) in O$_2$ but note that previous studies of k_5 close to the low-pressure limit indicate the same values of m for He, N$_2$, and Ar even though the third-body efficiencies of these three bath gases are very different (Anderson et al., 1974). There is no reason to expect that this would be different for O$_2$ and therefore do not consider the assumption of the same value of m for N$_2$ and O$_2$ to be a source of uncertainty in deriving rate coefficients for atmospheric conditions (i.e. a mixture of N$_2$ and O$_2$). We emphasize that, for use in atmospheric models, both the lower third body of efficiency of air compared to N$_2$ and the branching ratio to HNO$_3$ or HOONO formation need to be considered.

4 Conclusion

We report a new set of measurements of the rate coefficient (k_5) for the reaction of OH with NO$_2$ between 217 and 333 K and over a wide range a pressures in the fall-off regime in N$_2$ and O$_2$ bath gases. In order to measure NO$_2$ concentrations as accurately as possible we used three different optical absorption set-ups at different wavelengths/wavelength ranges as well as in situ, laser-induced-fluorescence detection of NO$_2$. The highly accurate and precise dataset obtained, combined with a theoretical value for the fall-off factor, enabled a more accurate assessment of the limiting low-pressure (k_0) rate coefficient than previous studies, including low-pressure flow-tube measurements. The rate coefficients we derive in the fall-off range are slightly larger than some previous studies using similar methods and the values for k_∞ are consistent with previous reports of this parameter based on experiments in high pressures of He and vibrational deactivation of OH in collision with NO$_2$.

We derive a parameterization of the overall rate coefficient and show that present divergent evaluations of k_5 result in significant differences, both underestimating and overestimating the rate coefficient in different parts of the atmosphere. Further study of the temperature and pressure dependence of the branching ratios on HNO$_3$ and HOONO formation as well as of the atmospheric fate of HOONO are required to fully understand and model the atmospheric impact of the title reaction.

References

Anastasi, C. and Smith, I. W. M.: Rate measurements of reactions of OH by resonance absorption. Part 5. – Rate constants for OH + NO$_2$ (+ M) → HNO$_3$ (+ M) over a wide range of temperature and pressure, J. Chem. Soc., Faraday T. 2, 72, 1459–1468, 1976.

Anderson, J. G. and Kaufman, F.: Kinetics of reaction OH + NO$_2$ + M → HNO$_3$ + M, Chem. Phys. Lett., 16, 375–379, 1972.

Anderson, J. G., Margitan, J. J., and Kaufman, F.: Gas-phase recombination of OH with NO and NO$_2$, J. Chem. Phys., 60, 3310–3317, 1974.

Anderson, L. G.: Absolute rate constants for the reaction of OH with NO$_2$ in N$_2$ and He from 225 to 389 K, J. Phys. Chem., 84, 2152–2155, 1980.

Atkinson, R., Baulch, D. L., Cox, R. A., Crowley, J. N., Hampson, R. F., Hynes, R. G., Jenkin, M. E., Rossi, M. J., and Troe, J.: Evaluated kinetic and photochemical data for atmospheric chemistry: Volume I – gas phase reactions of O$_x$, HO$_x$, NO$_x$ and SO$_x$ species, Atmos. Chem. Phys., 4, 1461–1738, https://doi.org/10.5194/acp-4-1461-2004, 2004.

Atkinson, R., Baulch, D. L., Cox, R. A., Crowley, J. N., Hampson, R. F., Hynes, R. G., Jenkin, M. E., Rossi, M. J., Troe, J., and IUPAC Subcommittee: Evaluated kinetic and photochemical data for atmospheric chemistry: Volume II – gas phase reactions of organic species, Atmos. Chem. Phys., 6, 3625–4055, https://doi.org/10.5194/acp-6-3625-2006, 2006.

Au, J. W. and Brion, C. E.: Absolute oscillator strengths for the valence-shell photoabsorption (2–200 eV) and the molecular and dissociative photoionization (11–80 eV) of nitrogen dioxide, Chem. Phys., 218, 109–126, 1997.

Brown, R. L.: Tubular flow reactors with first-order kinetics, J. Res. Nat. Bur. Sta., 83, 1–8, 1978.

Brown, S. S., Talukdar, R. K., and Ravishankara, A. R.: Rate constants for the reaction OH + NO$_2$ + M → HNO$_3$ + M under atmospheric conditions, Chem. Phys. Lett., 299, 277–284, 1999.

Burkholder, J. B., Sander, S. P., Abbatt, J., Barker, J. R., Huie, R. E., Kolb, C. E., Kurylo, M. J., Orkin, V. L., Wilmouth, D. M., and Wine, P. H.: Chemical Kinetics and Photochemical Data for Use in Atmospheric Studies, Evaluation No. 18, JPL Publication 15-10, Jet Propulsion Laboratory, Pasadena, available at: http://jpldataeval.jpl.nasa.gov (last access: August 2019), 2015.

Burrows, J. P., Wallington, T. J., and Wayne, R. P.: Kinetics of the gas-phase reactions of OH with NO$_2$ and with NO, J. Chemical Soc.-Faraday T. II, 79, 111–122, 1983.

Cobos, C. J. and Troe, J.: Prediction of reduced falloff curves for recombination reactions at low temperatures, Z. Phys. Chem., 217, 1031–1044, 2003.

Donahue, N. M., Dubey, M. K., Mohrschladt, R., Demerjian, K. L., and Anderson, J. G.: High-pressure flow study of the reactions OH + NO$_x$ → HONO$_x$: Errors in the falloff region, J. Geophys. Res.-Atmos., 102, 6159–6168, 1997.

D'Ottone, L., Campuzano-Jost, P., Bauer, D., and Hynes, A. J.: A pulsed laser photolysis-pulsed laser induced fluorescence study of the kinetics of the gas-phase reaction of OH with NO$_2$, J. Phys. Chem. A, 105, 10538–10543, 2001.

D'Ottone, L., Bauer, D., Campuzano-Jost, P., Fardy, M., and Hynes, A. J.: Kinetic and mechanistic studies of the recombination of OH with NO$_2$: Vibrational deactivation, isotopic scrambling and product isomer branching ratios, Faraday Discuss., 130, 111–123, 2005.

Dransfield, T. J., Perkins, K. K., Donahue, N. M., Anderson, J. G., Sprengnether, M. M., and Demerjian, K. L.: Temperature and pressure dependent kinetics of the gas-phase reaction of the hydroxyl radical with nitrogen dioxide, Geophys. Res. Lett., 26, 687–690, 1999.

Dulitz, K., Amedro, D., Dillon, T. J., Pozzer, A., and Crowley, J. N.: Temperature-(208–318 K) and pressure-(18–696 Torr) dependent rate coefficients for the reaction between OH and HNO$_3$, Atmos. Chem. Phys., 18, 2381–2394, https://doi.org/10.5194/acp-18-2381-2018, 2018.

Golden, D. M., Barker, J. R., and Lohr, L. L.: Master equation models for the pressure- and temperature-dependant reactions HO + NO$_2$ → HONO$_2$ and HO + NO$_2$ → HOONO, J. Phys. Chem. A, 107, 11057–11071, 2003.

Hippler, H., Nasterlack, S., and Striebel, F.: Reaction of OH + NO$_2$ + M: Kinetic evidence of isomer formation, Phys. Chem. Chem. Phys., 4, 2959–2964, 2002.

Hippler, H., Krasteva, N., Nasterlack, S., and Striebel, F.: Reaction of OH + NO$_2$: High pressure experiments and falloff analysis, J. Phys. Chem. A, 110, 6781-6788, 2006.

Howard, C. J. and Evenson, K. M.: Laser magnetic-resonance study of gas-phase reactions of OH with CO, NO, and NO$_2$, J. Chem. Phys., 61, 1943–1952, 1974.

Howard, C. J.: Kinetic measurements using flow tubes, J. Phys. Chem., 83, 3–9, 1979.

IUPAC: Task Group on Atmospheric Chemical Kinetic Data Evaluation, edited by: Ammann, M., Cox, R. A., Crowley, J. N., Herrmann, H., Jenkin, M. E., McNeill, V. F., Mellouki, A., Rossi,

M. J., Troe, J., and Wallington, T. J., available at: http://iupac. pole-ether.fr/index.html, last access: March 2019.

Keil, D. G., Donnelly, V. M., and Kaufman, F.: Fluorescence lifetime studies of NO_2. IV. Temperature dependence of fluorescence spectra and of collisional quenching of fluorescence, J. Chem. Phys., 73, 1514–1520, 1980.

Keyser, L. F.: High-pressure flow kinetics – A study of the OH + HCl reaction from 2 to 100 Torr, J. Phys. Chem., 88, 4750–4758, 1984.

Lelieveld, J., Dentener, F. J., Peters, W., and Krol, M. C.: On the role of hydroxyl radicals in the self-cleaning capacity of the troposphere, Atmos. Chem. Phys., 4, 2337–2344, https://doi.org/10.5194/acp-4-2337-2004, 2004.

Lelieveld, J., Gromov, S., Pozzer, A., and Taraborrelli, D.: Global tropospheric hydroxyl distribution, budget and reactivity, Atmos. Chem. Phys., 16, 12477–12493, https://doi.org/10.5194/acp-16-12477-2016, 2016.

Merienne, M. F., Jenouvrier, A., and Coquart, B.: The NO_2 absorption-spectrum. 1. Absorption cross-sections at ambient-temperature in the 300–500 nm region, J. Atmos. Chem., 20, 281–297, 1995.

Mollner, A. K., Valluvadasan, S., Feng, L., Sprague, M. K., Okumura, M., Milligan, D. B., Bloss, W. J., Sander, S. P., Martien, P. T., Harley, R. A., McCoy, A. B., and Carter, W. P. L.: Rate of gas phase association of hydroxyl radical and nitrogen dioxide, Science, 330, 646–649, 2010.

Newsome, B. and Evans, M.: Impact of uncertainties in inorganic chemical rate constants on tropospheric composition and ozone radiative forcing, Atmos. Chem. Phys., 17, 14333–14352, https://doi.org/10.5194/acp-17-14333-2017, 2017.

Nizkorodov, S. A., Sander, S. P., and Brown, L. R.: Temperature and pressure dependence of high-resolution air-broadened absorption cross sections of NO_2 (415–525 nm), J. Phys. Chem. A, 108, 4864–4872, 2004.

Orphal, J.: A critical review of the absorption cross-sections of O_3 and NO_2 in the ultraviolet and visible, J. Photochem. Photobiol. A, 157, 185–209, 2003.

Schurath, U., Lippmann, H. H., and Jesser, B.: Temperature dependence of the chemiluminescent reaction (1), $NO + O_3 \rightarrow NO_2(^2A_1; {}^2B_{1,2}) + O_2$, and quenching of the excited product, Berichte der Bunsengesellschaft für physikalische Chemie, 85, 807–813, 1981.

Smith, I. W. and Williams, M. D.: Vibrational-relaxation of OH($v = 1$) and OD($v = 1$) By HNO_3, DNO_3, H_2O, NO and NO_2, J. Chem. Soc. Faraday Trans. 2, 81, 1849–1860, 1985.

Troe, J.: Theory of thermal unimolecular reactions in the fall-off range 1. Strong collision rate constants, Berichte Der Bunsen-Gesellschaft-Physical Chemistry Chemical Physics, 87, 161–169, 1983.

Troe, J.: Refined representation of falloff curves for the reaction $HO + NO_2 + N_2 \rightarrow (HONO_2, HOONO) + N_2$, J. Phys. Chem. A, 116, 6387–6393, 2012.

Vandaele, A. C., Hermans, C., Simon, P. C., Carleer, M., Colin, R., Fally, S., Merienne, M. F., Jenouvrier, A., and Coquart, B.: Measurements of the NO_2 absorption cross-section from $42\,000\,cm^{-1}$ to $10\,000\,cm^{-1}$ (238–1000 nm) at 220 K and 294 K, J. Quant. Spectrosc. Ra., 59, 171–184, 1998.

Vandaele, A. C., Hermans, C., Fally, S., Carleer, M., Colin, R., Merienne, M. F., Jenouvrier, A., and Coquart, B.: High-resolution Fourier transform measurement of the NO_2 visible and near-infrared absorption cross sections: Temperature and pressure effects, J. Geophys. Res.-Atmos., 107, 4348, https://doi.org/10.1029/2001JD000971, 2002.

Wine, P. H., Kreutter, N. M., and Ravishankara, A. R.: Flash photolysis-resonance fluorescence kinetics study of the reaction $OH + NO_2 + M \rightarrow HNO_3 + M$, J. Phys. Chem., 83, 3191–3195, 1979.

Wollenhaupt, M., Carl, S. A., Horowitz, A., and Crowley, J. N.: Rate coefficients for reaction of OH with acetone between 202 and 395 K, J. Phys. Chem., 104, 2695–2705, 2000.

Yoshino, K., Esmond, J. R., and Parkinson, W. H.: High-resolution absorption cross section measurements of NO_2 in the UV and visible region, Chem. Phys., 221, 169–174, 1997.